Enhanced Tunable Terahertz-wave generation in Photonic Band Gap structures

Thesis

Submitted to

Graduate Engineering & Research

School of Engineering

UNIVERSITY OF DAYTON

In Partial Fulfillment of the Requirements for

The Degree

Master of Science in Electrical Engineering

By

Prasanth Kumar Bojja

UNIVERSITY OF DAYTON

Dayton, OHIO

December 2003

Enhanced Tunable Terahertz-wave Generation in Photonic Band Gap Structures

APPROVED BY:

Peter E. Powers, Ph. D.
Advisory Committee Chairman
Associate Professor, Physics and
Electro-Optics

Joseph W. Haus, Ph. D.
Committee Member
Director, Electro-Optics Graduate
Program

Guru Subramanyam, Ph. D.
Committee Member
Associate Professor, Electrical and
Computer Engineering

Donald L. Moon, Ph. D.
Associate Dean
Graduate Engineering Programs &
Research, School of Engineering

Blake Cherrington, Ph. D., P. E.
Dean
School of Engineering

ABSTRACT

ENAHNCED TUNABLE TERAHERTZ-WAVE GENERATION IN PHOTONIC BAND GAP STRUCTURES

Name: Bojja Prasanth Kumar
University of Dayton, OHIO

Advisor: Dr. Peter E. Powers

This thesis explores generating enhanced tunable terahertz-wave based on parametric down-conversion in Photonic Band Gap (PBG) structures. Our design is based on the band edge or defect-mode field enhancement phenomena near a photonic band gap. Calculations demonstrate that the enhancement values enable us to obtain narrow-band, continuously tunable terahertz (THz) sources from sub-THz to 12 THz with power levels around 10 μW using 1 W continuous-wave (cw) lasers. Analysis demonstrate that a wide range of intensities and bandwidths of coherent radiation can be obtained as we vary either the number of periods or the index contrast between layers of the PBG crystal array. The laboratory setup for developing the source for THz wave generation using the optical parametric generation (OPG) and finally the detection setup using the bolometer is presented.

ACKNOWLEDGEMENTS

It gives me great pleasure to acknowledge my indebtedness and a deep sense of gratitude to my respected advisor Dr. Peter E Powers, Associate Professor, Department of Physics and Electro-Optics, for his guidance. He has been a constant source of inspiration and had helped me at each step. Under his guidance I learned about the nonlinear optics and successfully overcome many difficulties in the lab. His idea of working on various projects in the lab besides my research topic and the discussions in the lab enhanced my knowledge and interest in nonlinear optics. I express my deep gratitude to him for being extremely considerate and patient with me in listening to my problems time and again. Without his help this thesis work wouldn't have been completed.

I want to thank Dr. Joseph Haus for encouraging me to participate in this research. He not only provided me with equipment, and funding, but he also helped me to understand the behavior of the Photonic Band Gap structures. He also served on my advisory committee despite his busy schedule. Without his help the modeling and analysis discussed in this thesis could not have been put together.

I want to thank Dr. Miguel Torres-Cisneros for helping with the thin film optics behavior studies. I also want to thank Dr. Guru Subramanyam for being on

my advisory committee and helping in understanding the basics of the microwave testing using vector network analyzer.

I want to express my appreciations to the faculty and staff of Electrical and Computer Engineering, Physics, and Electro-optics at the University of Dayton, especially to Dr. Partha P. Banerjee, Dr. John S. Loomis, Dr. Perry P. Yaney, and Dr. Andrew Sarangan. Special thanks to Trina Downs for always making sure that my paper work was straight and turned in on time. I want to thank my friends for their encouragement and support, especially Raghu, Ramesh, and Santhosh. I also want to thank the many other University of Dayton students for their help, especially Yi Yi, Eric, Rashid, Vilas, Vikram, Charan, and Srinivas.

Finally, I would like to express my deepest gratitude to the most important people in my life, my family, especially my parents - Swarnakumari and Chandramouli, and my sister - Swarupa for their constant support, understanding, and love that I received.

This research work is supported in part by the Electro-Optics department at the University of Dayton (OH), a grant from National Science Foundation, and ITT Industries.

Prasanth Bojja

November 04, 2003

TABLE OF CONTENTS

LIST OF FIGURES

Chapter 1
Introduction

Generation of the coherent sources in microwave and in visible regions is the interesting area of research for scientific, commercial, and military applications. Tunable, reliable, compact, and economical THz sources are not readily available. Several techniques have been developed based on either novel schemes or exploiting well-known effects inorder to develop the THz sources. Each of these designs has different characteristics and works potentially in a range of the wide THz region [0.1 – 10 THz]. In this thesis, we report the modeling and laboratory development of one of the important techniques of THz-wave generation based on parametric down-conversion in a photonic crystal. Our calculations demonstrate the generation of signals from sub-THz to more than 12 THz and power levels around 10μW using 1W cw lasers. Both the bandwidth and intensity of the signal can be tuned by varying the number of layers, the refractive index contrast of the PBG sample or angle tuning the fields between two spectrally separated transmission resonances or defect modes.

Photonic crystals are periodic dielectric structures that have a band gap that forbids propagation over a certain frequency range of light. There are many optical properties of photonic crystals that enable control of light with amazing facility and produce effects that are not possible with conventional optics. A

simple one-dimensional Photonic Band Gap (PBG) structure consists of a multi-layer array with several periods deposited on a substrate.

In Chapter 2, we discuss the modeling of the enhanced tunable terahertz-wave generation in PBG crystals, we demonstrate the effects of the number of layers, the refractive index contrast, and the angle tuning of the input fields on the bandwidth and intensity of the signal. We also present the THz power conversion. Chapter 3 discusses about the THz-wave generation laboratory setup. This chapter covers the operation and building of the Injection seeded diode pumped Nd:YVO_4 pump laser system, Optical Parametric Generation (OPG) setup, and the detection of the generated THz signal using the Si-bolometer. Finally, Chapter 4 summarizes the work presented in this thesis and many promising areas of research that follow this work.

Chapter 2
Modeling of Enhanced Tunable Terahertz-wave Generation in Photonic Band Gap Structures

2.1 Introduction

Applications of coherent terahertz (THz) sources in millimeter wave imaging, spectroscopy, and others have increased the interest to find a compact, tunable, reliable, and economic new designs. Several approaches are available for THz sources. The passive solid-state[1] source design is one of the best proposals for the low portion of the THz spectrum but spectral coverage is limited. Other promising designs involve optical effects as photoconductivity (PC)[2,3], optical parametric oscillation[4,5] (OPO), optical parametric generation (OPG)[6], optical rectification[7,8,9,10], photomixing[11,12], and femtosecond pulse shaping[13]. Quantum cascade lasers[14] form another branch of active THz device development. These sources can generate THz frequencies with output powers ranging from nanowatts to milliwatts.

Some THz sources are currently applied to specific technologies such as coherent time-domain spectroscopy[15], T-wave imaging and ranging of objects[16,17], dynamic analysis in semiconductors[18,19], environment monitoring[20], and frequency standards[21]. Novel concepts have been proposed for potential applications to radar systems, optical communications, medical imaging, nonlinear spectroscopy and so on. These applications would be enabled by

availability of the THz sources. The sources must satisfy different criteria, depending on the specific application, such as being compact, tunable across a wide portion of the THz bands, variable bandwidth, high power, and economical.

Recently, Yan-qing Lu and co-workers[22] proposed the use of a nonlinear photonic crystal (PBG) to generate coherent microwave radiation. They used the PBG characteristics in order to solve the phase-matching problem. In this chapter, we demonstrate the numerical analysis for the generation of THz using a PBG structure but focusing on the band-edge and defect effects. The phenomena involved in these THz regions are field enhancement and increase density of states or slow group velocity of the optical wave[23]. All these can provide great flexibility in the THz wave generation. We have looked at several geometries using GaAs, as the first material and materials as AlAs, Al_2O_3 (alumina) or air as the second material. Each pair provides a larger index contrast.

2.2 Theoretical Analysis

The theoretical analysis or modeling based on the matrix method using Fresnel coefficients as described in the reference [24] is used to compute the fields at two wavelengths inside the PBG structure that are detuned from one another to generate the desired difference frequency. Both driving fields are tuned near the same transmission resonance in the structure. The number of periods, the dispersive dielectric properties of the materials, thickness of the layers and the substrate details were incorporated in to the program. THz signal

enhancement is determined by taking the products of two fields in the sample, located at different wavelengths, integrating over the sample and normalizing with respect to the nonlinear length. THz Power conversion is explained in section 2.5 on THz power conversion.

2.3 Band-edge Enhancement

One of the local-field enhancement mechanisms is tuning the driving fields to the band-edge. A simple one-dimensional PBG sample consists of a multi-layer array with m periods deposited on a substrate, as shown in Figure 2.1. Each period in the PBG structure consists of one layer of GaAs and one layer of AlAs; both a quarter-wave thick i.e. the thickness of each layer was chosen to be a quarter wavelength of the light at the center of the band gap. A GaAs substrate is used, but we also explored eliminating the substrate and using an air interface on each side for comparison.

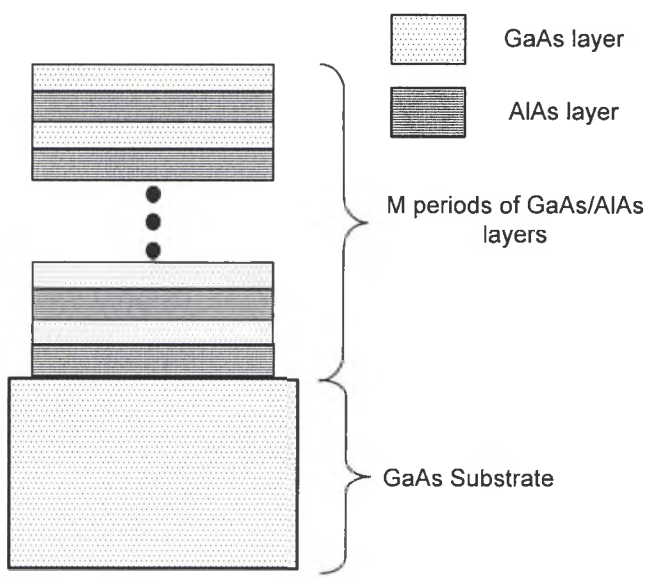

Figure 2.1- Geometry array: m GaAs/AlAs periods deposited on a GaAs substrate. Each period consist of one GaAs layer followed by a second, lower-index material, i.e. we consider (AlAs, Al_2O_3, air) layer. The substrate thickness is assumed to be infinite.

The calculated transmission spectra for GaAs/AlAs quarter wavelength PBG stack of 30 periods (60 layers) are shown in Figure 2.2. The design was chosen in such a way that the transmission peak on the long-wavelength edge of the band gap is close to one micron. In Figure 2.2a the GaAs substrate supports the PBG structure, and in Figure 2.2b the substrate is removed. The layers thicknesses are d(GaAs) = 71.42 nm and d(AlAs) = 85.94 nm. The transmission spectra show that the large refraction index contrast for the air-substrate case generates higher transmission peaks. Correspondingly, calculation of the local fields in the structure when the field is tuned at the first transmission resonance reveals that the GaAs-substrate has smaller resonant-field values in the PBG. The substrate affects the efficiency of the final THz device design, as is demonstrated below.

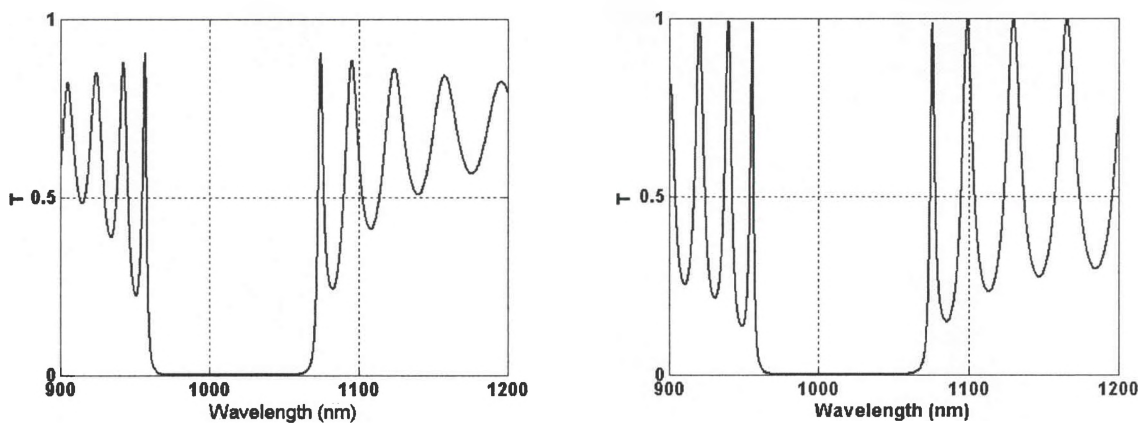

(a) GaAs substrate

(b) Air Substrate

Figure 2.2 - Plots of the transmission spectra for 30 periods (60 layers) illustrate the effect of the substrate. Physical parameters are described in the text. The two materials are GaAs/AlAs on a, (a) GaAs substrate. (b) Air substrate.

The maximum values in these transmission peaks are reached at 1074.4 nm for the GaAs substrate and 1075.7 nm for the air substrate case. The wavelength is tuned to the first transmission resonance on the long wavelength side of the band gap obtained from the transmission spectra to get the electromagnetic field amplitude for both the substrate cases as shown in Figure 2.3. The GaAs substrate PBG structure has smaller field values and in both cases, the envelope of the field has a single maximum. For both cases the field enhancement is modest, but the maximum increases rapidly as more periods are added to the PBG. Also we demonstrate below large enhancements are possible with added layers and when a defect is sandwiched between a pair of PBGs.

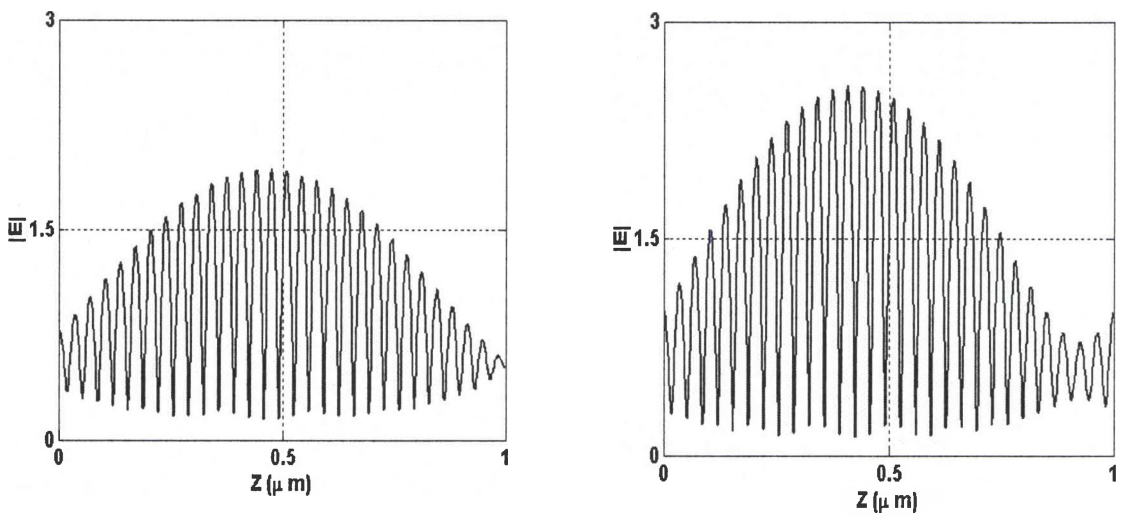

(a) 1074.4 nm (b) 1075.7 nm

Figure 2.3 - The field amplitudes in the PBG. a) GaAs substrate. b) Air substrate. The wavelengths of the fields were chosen at the first transmission on the long wavelength side of the band gap. The transmission maximum is different for the two cases: a) 1074.4 nm and b) 1075.7 nm.

Two coherent fields are mixed in a second-order nonlinear material to generate THz radiation. The down-converted output signal is proportional to the

product of the two fields inside the PBG sample. The thickness of the sample is much smaller than the wavelength of the down-converted signal and propagation effects can be neglected, this also eliminates the need for phase matching the fields. By taking the product of the fields at different wavelengths and integrating over the sample we determine the sub-THz signal enhancement, which is expressed as

$$\eta = \frac{\left| \int_0^L E_1 E_2^* dz \right|^2}{L^2} \tag{1}$$

The enhancement for GaAs and air substrates are as shown in Figure 2.4, both laser sources are normally incident on the PBG sample. The wavelength of one laser is fixed at the transmission maximum and the second laser is continuously tuned around the transmission maximum. The maximum enhancement occurs near the degeneracy frequency of the two lasers, since the overlap of the field profiles is perfect. As the second laser is detuned the overlap changes in both amplitude and phase, and sharply reduces the enhancement. The field enhancement peak does not occur when both lasers are tuned to the same frequency (one laser remains tuned on the transmission maximum) because the maximum of the density of states is shifted slightly from the transmission maximum and this is manifest by a slight increase in the energy stored inside the PBG.

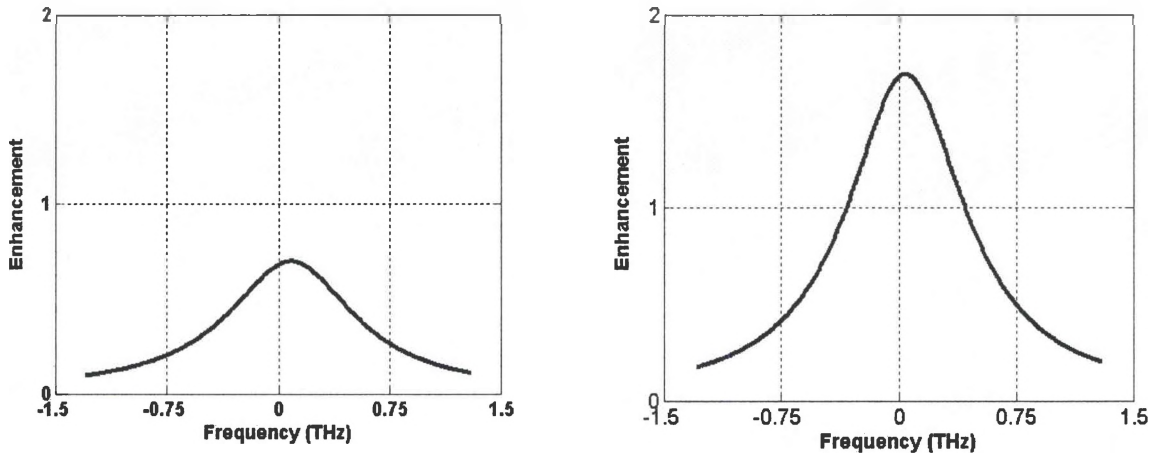

(a) GaAs substrate

(b) Air Substrate

Figure 2.4 - Down-converted enhancement obtained for the samples from the field amplitudes in Figure 2.3; the two cases are: (a) GaAs substrate and (b) air substrate.

Equation (1) for the enhancement considered is a crude measure that assumes a second-order nonlinearity to be the same in both materials. The normalization is the expected low-frequency signal when the sample is perfectly phase matched in the homogeneous sample of the same length and same nonlinear coefficient. We have also extended this to the case when the second material does not possess a second-order nonlinear optical response to cover the alumina and air layer cases. In those samples equation (1) is modified so that the integral only extends over the GaAs layers.

The calculated enhancement is small in both the cases as shown in the Figure 2.4. Enhancement when GaAs is used as substrate is about 58% smaller than the air-substrate. The bandwidth of the resonance is nearly 1 THz. As the number of periods is increased the enhancement rapidly increases; however, on the other hand the bandwidth of the resonance also decreases as more layers are added.

The band-edge enhancement for 20 and 30 periods is as shown in the Figure 2.5, In this case the index of refraction for the second layer is changed but the thickness of each layer is the same as the previous examples: d(GaAs) = 71.42 nm and d(Al_2O_3) = 85.94 nm. The layer pairs are GaAs/Al_2O_3 with air for both the substrate and superstrate. For 40 layers (i.e. 20 periods), the THz signal enhancement is about 35; further increasing the number of layers by 50% results in an increase of the peak signal enhancement of about a factor of four.

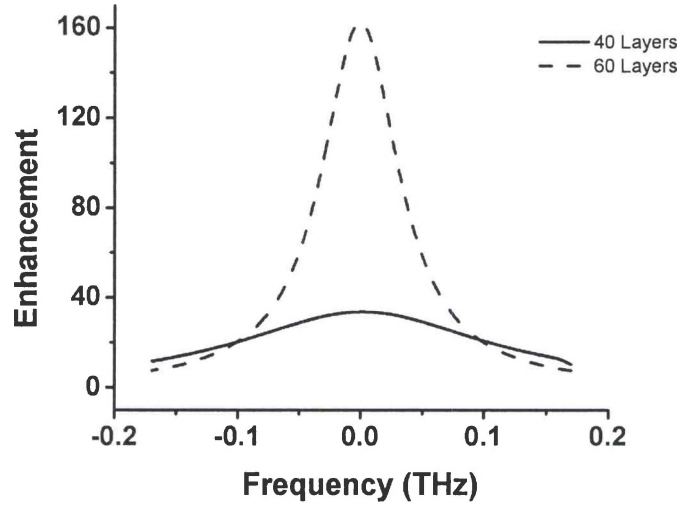

Figure 2.5 - Band-edge enhancement versus frequency plotted for two cases: 20 and 30 periods. In this case a larger index contrast was used; each period is composed of GaAs/Al_2O_3 layers, Refractive index of GaAs is 3.374 @ 1.5μm and Al_2O_3 is 1.5 @ 1.4 μm; the GaAs substrate is removed. The other parameters are identical to those used in Figures 2.2 through 2.4. Note the two orders of magnitude difference in the enhancement intensity (against Figure. 2.4b case) obtained by increasing the index contrast.

Comparing the enhancement intensities for the same number of layers (30) but for different index contrast, i.e. GaAs/AlAs Figure 2.4a and GaAs/Al_2O_3 the Figure 2.5, larger enhancements are achieved with a greater index contrast, but the resonance bandwidth is also narrower. Substituting Al_2O_3 (1.5 @ 1.4 μm)

for AlAs (2.919 @ 1.378 μm) produces more than an order of magnitude increase of the enhanced intensity for the same number of layers. From the curves in Figure 2.5, we get a reciprocal relation between the enhancement and the bandwidth: as the peak enhancement increases the bandwidth decreases. Using the same physical parameters as in Figure 2.5, the behavior of the bandwidth and enhancement versus the number of layers is plotted in Figure 2.6. It is observed that the enhancement is achieved at the cost of bandwidth. For about 40 layers the bandwidth is around 250 GHz reduced to a value around 71 GHz for 60 layers. We also found a sharper transmission spectrum and a larger field amplitude resonant enhancement.

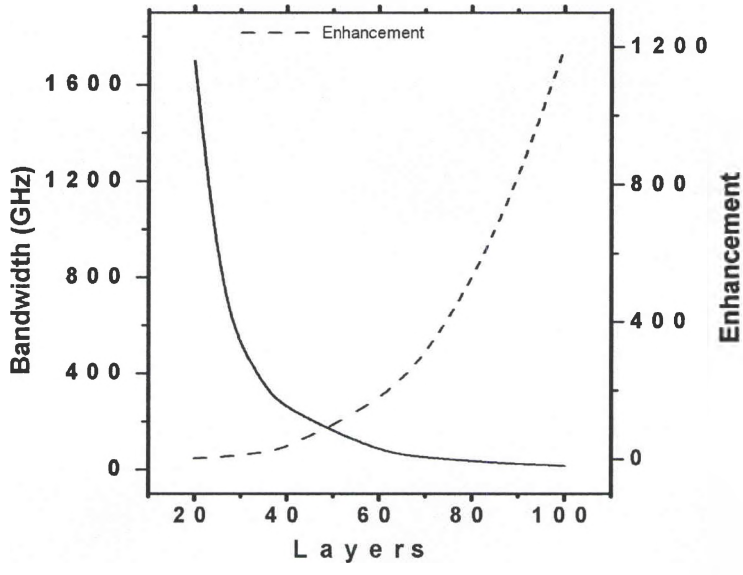

Figure 2.6 - Down-conversion signal enhancement versus the number of layer pairs for $GaAs/Al_2O_3$ PBG's. The parameters are the same as in Figure. 2.5.

In both illustrative examples, the signal enhancement only includes the GaAs material. The field enhancement is much larger than in Figure 2.4b. Thus fewer layers of high refractive index contrast materials are needed to achieve

greater down-converted signal enhancement. For instance, we find that 7 GaAs/Air periods (14 layers) has nearly the same signal enhancement as 30 GaAs/AlAs periods (60 layers) and it has a broader bandwidth. In order to determine the substrate effect on the field enhancement, a 14 layer GaAs/Air stack was placed on a GaAs substrate. There was little effect on the enhancement; although the choice of the substrate material is still relevant, it does not have the same importance as when the dielectric contrast between layers is smaller.

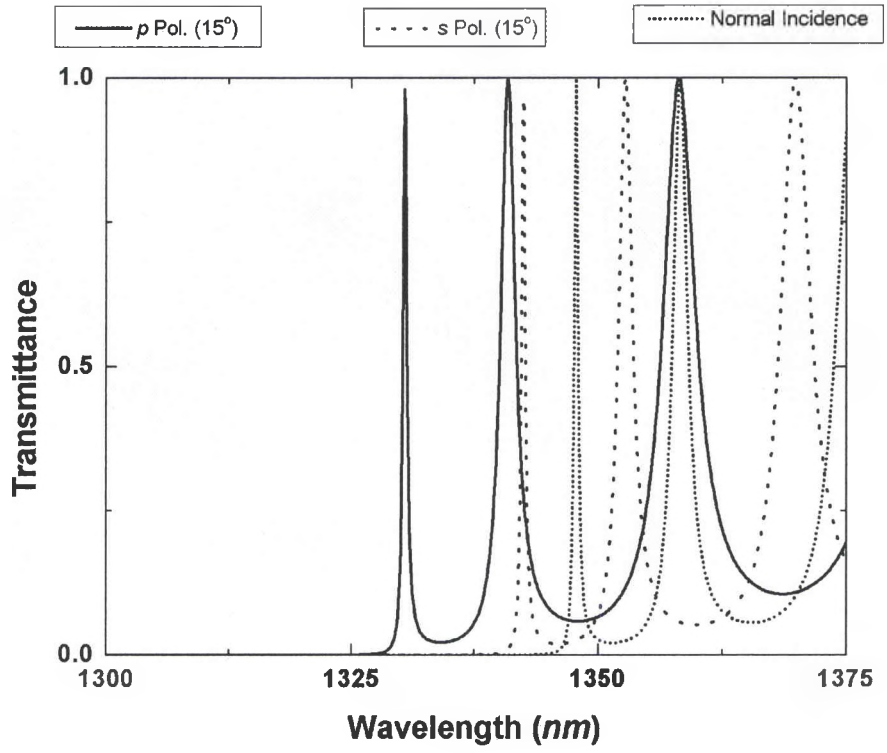

Figure 2.7 - Transmission spectra for normal incidence and 15 degree angle of incidence. The p- and s-polarizations have different shifts of their band-edge resonance peaks, but the resonance width is nearly the same.

The down-conversion frequency can be tuned by using two non co-linear laser sources. One laser is normally incident and the second laser is non-

normally incident, which shifts the transmission maximum and the band edge. Transmittance is calculated for normal, and the p- and s- polarizations incident at an angle of 15 degrees from the normal using the same parameters as for the dashed curve in Figure 6 (N=60, d(GaAs) = 71.42 nm, $d(Al_2O_3)$ = 85.94 nm). The transmission spectra are as shown in the Figure 2.7. At non-normal incident angles the transmission spectrum is different for p- and s- polarizations. For the same angle of incidence we find that the p-polarization has a much larger shift than the s-polarization. For both cases the width of the resonances and the field enhancement inside the PBG structure is similar.

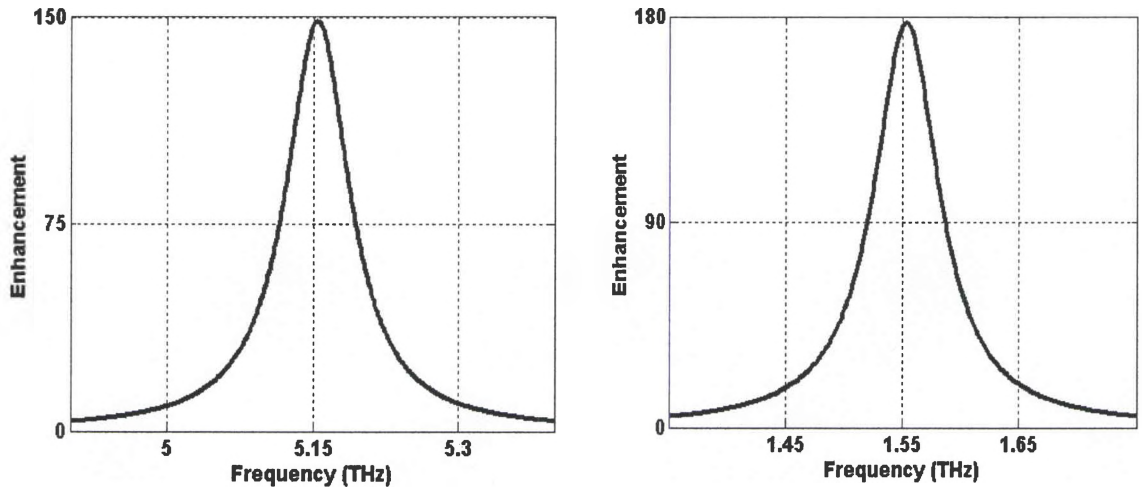

(a) p-polarization (b) s-polarization

Figure 2.8 - Resonance enhancement of the THz signal for (a) p-polarization and (b) s-polarization. The peak is shifted into the THz regime and the resonance width remains narrow.

Figures 2.8a and 2.8b show that the overlap of the two fields is excellent and the enhancement is 150 and 180 for p- and s-polarizations, respectively. The p-polarization has a maximum enhancement frequency at 5.15 THz, while for s-polarization the maximum is at 1.55 THz. Figure 2.9 highlights our results on the dependence of the THz emission with the angle tuning. The polarizations are

degenerate at normal incidence and have their maximum near 0 frequency. By changing the angle of incidence of one laser to 30 degrees the signal frequency at the maximum enhancement is about 11.5 THz for p-polarization and 3.5 THz for s-polarization. The peak enhancement for both polarizations remains over two orders of magnitude. The bandwidth of the enhancement peaks remains around 75 GHz over the entire range of angles.

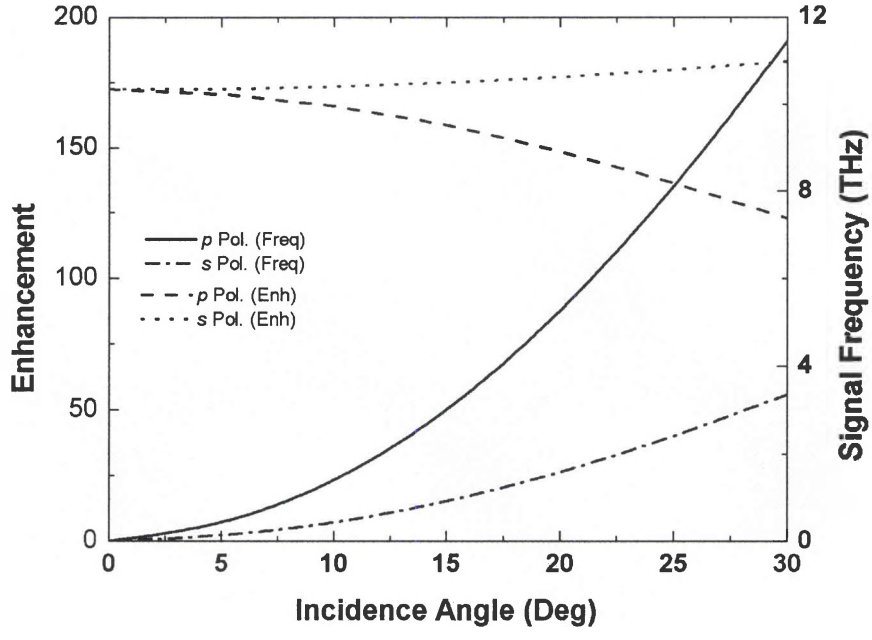

Figure 2.9 - Enhancement and signal frequency versus angle of incidence for p- and s-polarizations.

2.4 Defect Enhancement

A defect in the PBG crystal breaks the usual periodicity of the crystal, which can support modes that lie inside the band gap of the bulk crystal, and that these modes are localized in the vicinity of the defect.[25] A localized defect mode can also be exploited as a mechanism to enhance THz signals in a PBG structure. A defect mode is established by placing a layer that is some multiple

of a half-wave layer thickness between the quarter-wave multi-layer stacks. Figure 2.10 illustrates the sample geometry of the PBG structure with a defect mode and GaAs as substrate for this case. The number of layers sandwiching the defect are not necessarily the same. The defect enhancement is very sensitive to the number of layers as the band-edge enhancement case.

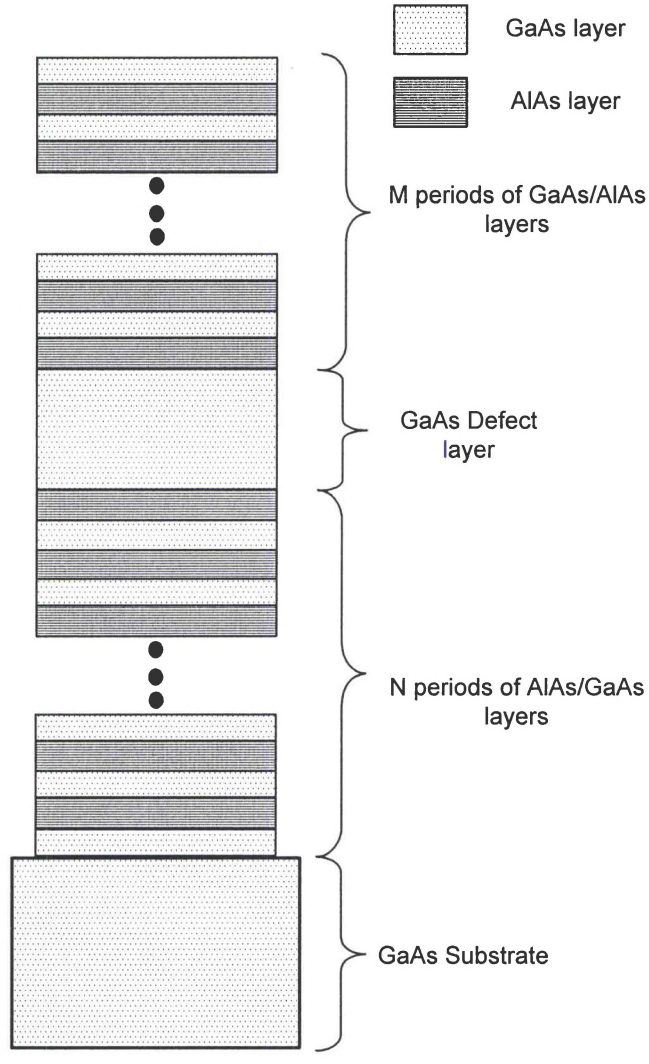

Figure 2.10 - Sample geometry with a defect layer sandwiched between two PBG stacks. The top PBG stack has M periods and the bottom stack has N periods. The defect layer and the substrate are GaAs.

For calculating the transmission and the enhancement, we have chosen the parameters of an available PBG sample that was used for a different

experiment. The parameters are: M=18 periods of GaAs/AlAs layers (top stack) and N=22 periods of AlAs/GaAs layers (bottom stack), each period is made of two quarter-wave thickness layers. The thickness of the GaAs layers is 112.42 nm and 130.45 nm for the AlAs layers. The GaAs defect layer has a thickness of 1349 nm and the substrate is infinitely thick. The gap lies in the infrared region, it extends from 1400-1700 nm. Figure 2.11 shows the transmission spectrum for the sample at normal incidence. A defect mode is present in the center of the gap. The transmission curve is very sharp at the defect mode position, which peaks at 1518.87 nm. The plot is chosen with a 0.05 spacing grid, at defect mode the points are spaced by 0.01 nm. The defect mode in the center is sharp and has a large Q-factor. The transmission through this PBG crystal measured in the lab using tunable cw diode laser from 1517nm-1519.5nm (0.1nm step is used between 1518 and 1519 to look at the defect mode) is shown in the Figure 2.12. The transmission spectrum from the model and lab has a defect mode around 1518.5nm but conflict in % transmission (this difference can be from the position of the incidence on the PBG sample or the angle of incidence). The local field distribution when driving laser's wavelength is tuned to the maximum transmission at the defect is shown in Figure 2.13. The resonant intensity is increased by two orders of magnitude.

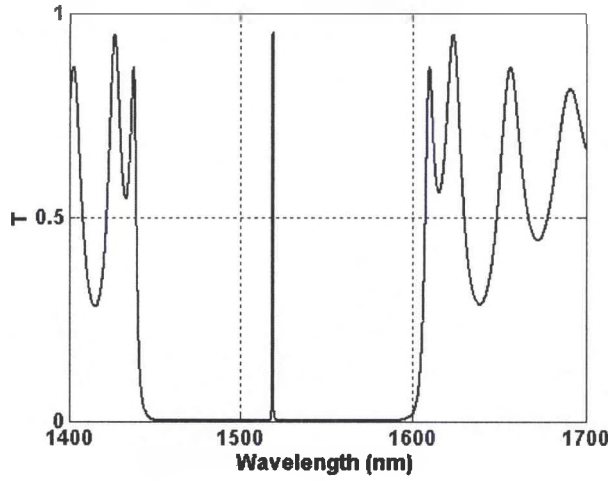

Figure 2.11 - Transmission spectra using the model for GaAs/AlAs sample with defect mode shown in the band gap.

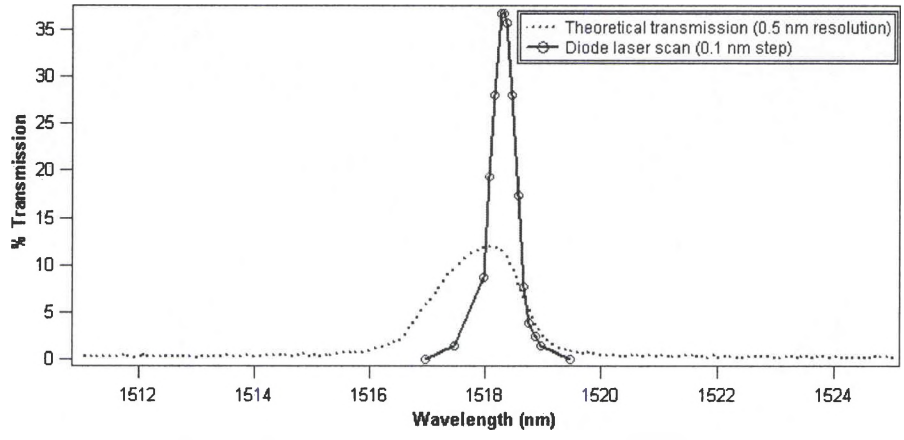

Figure 2.12 - Transmission spectra: Theoretical and that measured in the lab using tunable cw diode laser for GaAs/AlAs sample with defect mode.

At normal incidence the magnitude of the enhancement for this case is about 550. This is almost three orders of magnitude enhancement over the band-edge enhancement case shown in Figure 2.4. The resonant width of the enhancement peak is about 40 GHz, which is wide enough to minimize the laser bandwidth effects. By angle tuning one laser we again observe a shift of the resonance position for both polarizations. The shift is much smaller for this defect example than it was for band-edge case discussed earlier. Figure 2.14 shows the enhancement versus tuning frequency for 30 degrees angle of incidence. At 30

degrees angle of incidence the peak enhancement occurs at 2.3 THz, magnitude of enhancement is 420 for the p-polarization, the s-polarization shift is similar to the p-polarization shift in this case. The bandwidth is very narrow. By using larger angles of incidence the frequency can be increased, but remains well below 10 THz out to angles of incidence of 80 degrees.

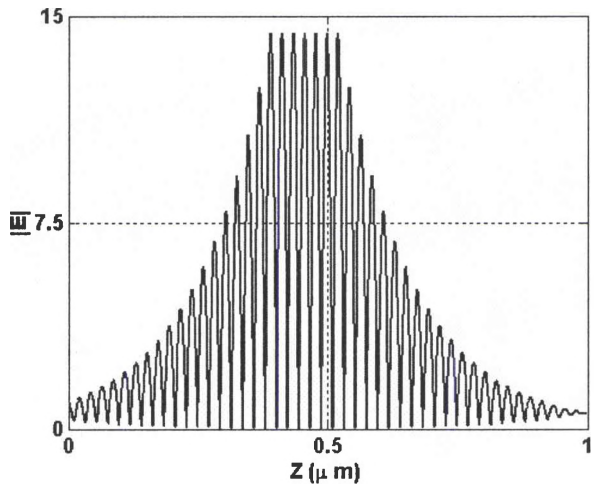

Figure 2.13 - The field amplitude in the PBG at the peak of the defect-mode transmission shown in Figure11.

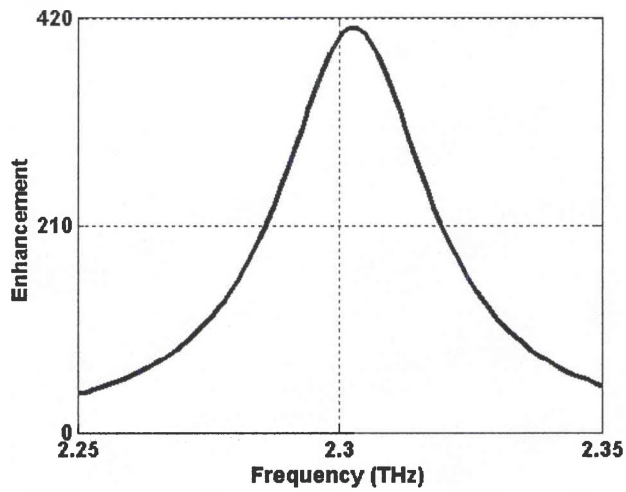

Figure 2.14 - Signal enhancement versus frequency. The angle of incidence of the second laser is 30 degrees. Only p-polarization is shown here.

2.5 THz Power Conversion

The power conversion efficiency can be roughly estimated for this process. The laser intensity (I) and the THz (I_{THz}) intensity in free space is expressed in MKSA units as

$$I = \frac{c\varepsilon_0}{2} |E|^2 \tag{2}$$

Driving the THz signal with 1 mW of signal power focused to a spot area of 10^{-3} cm^2 yields electric field (E) amplitude around 0.2×10^4 V/m where c is 3×10^8 m/s and ε_o is 8.85×10^{-12} F/m. The THz field generated in the PBG is estimated from an approximate coupled-mode equation, whose expression is

$$E_{THz} = \frac{2\pi}{\lambda} \chi^{(2)} \int_0^L E_1 E_2^* dz \tag{3}$$

The THz intensity is given by

$$I_{THz} = \frac{c\varepsilon_0}{2} \left(\frac{2\pi}{\lambda} L \right)^2 \eta \left(\chi^{(2)} |E|^2 \right)^2 \tag{4}$$

For our estimate of the conversion efficiency we use: a sample length: L=10 μm, generated frequency: ν=1 THz or λ=300 μm, $\chi^{(2)} = 10^{-11}$ m/V, $\eta=10^2$, and $E1$ and $E2^*$ correspond to the incident fields. The THz power generation is about 10 pW. The result scales proportional to the pump power; so for 1 W laser powers the THz signal will be about 10 μW. The overall efficiency is inversely proportional to the THz wavelength, so higher frequencies will be generated with

higher power. A large portion (more than two orders of magnitude) of the power inefficiency is due to the quantum efficiency of the down-conversion process.

2.6 Summary

We demonstrated that tunable, enhanced, long-wavelength signal generation from sub-THz to several THz is attainable using either band-edge or defect effects in a second-order nonlinear PBG. By designing samples with specific numbers of layers and refractive index contrast we can tune both the bandwidth and intensity of the signal. The excitation wavelengths are determined solely by the thickness of the layers. For low refractive index materials the signal enhancement increases by an order of magnitude for the same number of layers. The enhancement grows as the number of layers is increased; however, the bandwidth of the resonance also decreases as more layers are added. The final optimized structure does not rely on GaAs for the nonlinear mixing to generate radiation. Other materials such as, GaN or even poled electro-optic polymers could be incorporated into final designs, based on the availability of fabrication techniques. We also find that a defect-mode is very effective providing large intensity enhancements, although the shift is not as large as the band edge resonances. For our case both p- and s-polarizations the defect mode shifts by the same amount.

The enhancement values could enable us to obtain signals with GHz to THz frequencies and power levels around 10 μW using 1 W cw lasers. The efficiency is enhanced over a small range typically tens of GHz; however, a

larger tuning into the THz range is achieved by angle tuning the fields between two spectrally separated transmission resonances or defect modes.

Chapter 3
Tunable Terahertz-Wave Generation Laboratory Setup

3.1 Introduction

Coherent THz-Waves are useful for a variety of scientific, commercial, and military applications. Various functions performed by the THz radiation sources are THz imaging, THz spectroscopy, wireless communications, and millimeter wave radar, just to name a few. Currently, there are various methods of generating THz waves, in the past using the ultra fast laser pulses, weak terahertz beams were generated. The weak terahertz beams are due to the absorption losses in the nonlinear medium. One recent method of great attention to achieve coherent, tunable, and powerful THz beams is using parametric processes like difference frequency generation (DFG) in a nonlinear medium of low absorption coefficient. In this method the difference between the two laser sources determines the frequency of the generated THz radiation. Thus generated radiation can be tunable if one or both of these laser sources are tunable.

Kawase *et. al* demonstrated tunable THz generation by difference frequency generation (DFG) of dual signal-wave quasi-phase matched optical parametric oscillator with periodically poled $LiNbO_3$ (PPLN) with a series of gratings in a 4-dimethylamino-N-methyl-4-stilbazolium-tosylate (DAST) nonlinear crystal. [26, 27] Ideally, one would like two independently tunable sources for the

difference frequency set up. Ding *et al.* demonstrated continuously tunable, and coherent terahertz radiation based on collinear phase-matched difference frequency generation separately in a GaSe crystal[28] and $ZnGeP_2$ crystal[29] (GaSe has the lowest and $ZnGeP_2$ has the next lowest absorption coefficient in the THz wavelength region). We are implementing a similar scheme as demonstrated by Ding *et. al.* except our source is easily tunable and has a high repetition rate (1 kHz). The two difference frequency sources used here are from two optical parametric generators (OPG). The OPG, when pumped with nsec pulses, has high conversion efficiency from a pump laser to the output signal and idler frequencies (roughly 20%). The output frequency is tunable by changing the crystal periodicity or temperature. To control the bandwidth of the OPG one injects a narrow bandwidth seed with the pump.[30] In our setup we use two diode lasers as the seed sources. The output of these two OPG's results in narrow linewidth centered at the diode laser frequency. By tuning the diode laser we then tune the two OPG's and our goal of two independently tunable sources is realized.

Generating the THz requires a nonlinear optical medium for DFG. In our method we have used the novel approach of using a one-dimensional photonic band gap (PBG) crystal as nonlinear optical medium. The two signal beams are focused on to the PBG crystal. Our calculations as per the model presented in chapter 2 show that THz radiation from sub-THz to more than 12 THz will be generated out of the PBG structure.

In this chapter, we describe the building and basic operation of the source for the THz-wave generation. This involves three stages. The first is the construction of a diode-pumped solid-state Nd:YVO_4 laser based on the design described by A. J. Alcock and John E. Bernard[31]. The second stage is the OPG setup, and the third is the detector setup.

3.2 Construction and basic operation of Nd: YVO_4 Laser System

In order to make the DFG set up we needed to construct the pump laser. This laser provides sufficient energy to drive two OPG stages (so that we can use the outputs for THz generation) and it operates at 1 kHz. The high repetition rate will be of great utility for signal averaging and general THz measurements. Other lasers available in the laboratory will only operate at low repetition rates. For this reason, we constructed a new high-repetition rate laser. The basic operation of Nd:Vanadate laser system can be divided in to diode pumping, cavity design, and Q-switching.

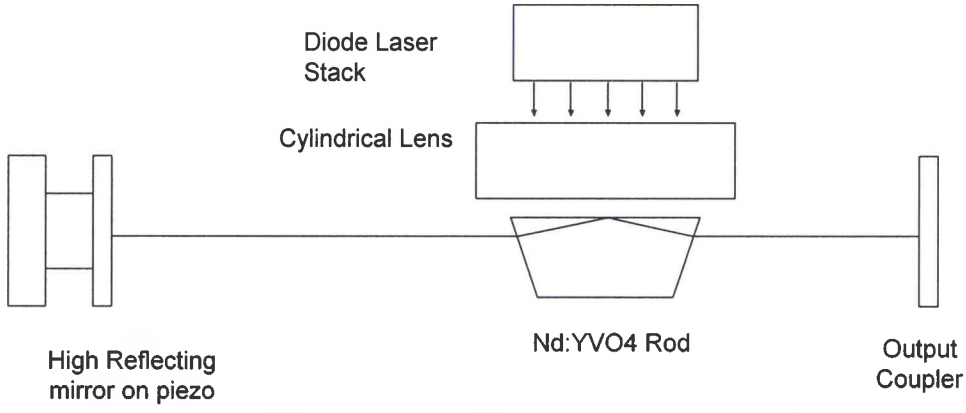

Figure 3.1 - Experimental arrangement of the diode side pumped Nd:YVO_4 cavity

The diode pumping and the cavity arrangement are similar to that described in [32] and [33]. The diode side-pumping arrangement is shown in the

Figure 3.1. It has five-bar diode laser stack (IMC model SDL-3231-G5) as pump source with a cylindrical microlens array which collimates the output perpendicular to the Nd:Vanadate Slab. The diode pump laser has a wavelength of 809nm driven by the driver (Analog Modules Inc Model 779A laser diode driver), diode pump laser produces a peak power of 200 W at a drive current of 70 amps. The collimated output of the cylindrical microlens array is focused onto a slab with a 10x5 mm (Width x Height) cylindrical lens onto the vanadate surface, with a polarization parallel to the vanadate c-axis. A Nd:YVO_4 slab of dimension 15 mm x 2 mm x 2 mm (Width x Depth x Height) is used as the gain element. The slab crystal-field energy levels and laser properties are explained in [34]. The slab end faces are polished, wedged, and antireflection coated for 1064nm at 0^o. The wedge angle is used to prevent an etalon parallel to the vanadate face. It also is used to facilitate a total internal reflection for the lasing mode. The lasing mode outside of the crystal is parallel to the vanadate face, when it enters the crystal through the wedged face, it is deflected such that it is at a grazing incidence with the vanadate face. This provides a good overlap with the gain while providing for a higher quality beam profile. Further details on this geometry and its benefits can be found in reference [35].

The cavity is formed between the end high reflecting mirror and the output coupling mirror. The output coupler is simply a Fresnel reflection off of a glass substrate. This low reflectivity is sufficient since the gain of the vanadate is so high. The cavity modes are dominated by the pumping because the end

mirrors are flat. Experimental arrangement of the side diode pumped Nd:Vanadate laser system as shown in the Figure 3.2.

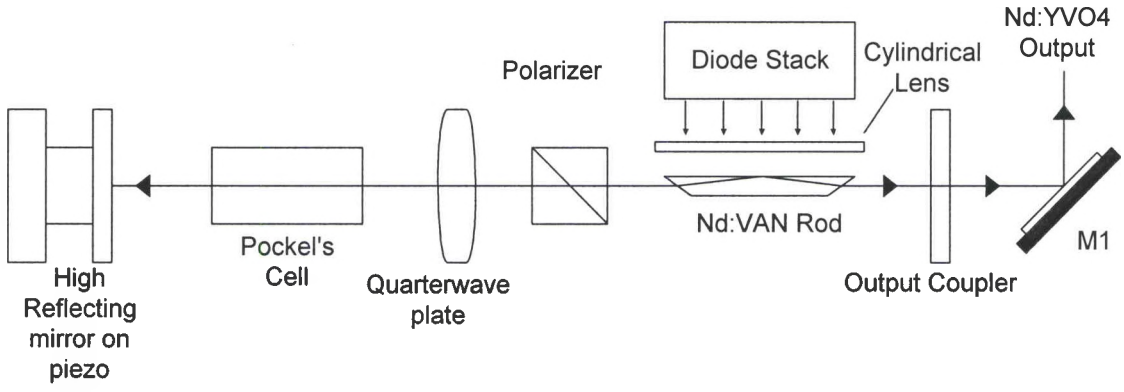

Figure 3.2 - Experimental side diode pumped Nd:YVO_4 laser system arrangement

The intracavity components of the Nd:Vanadate laser system are polarizer, Pockels cell, and quarter waveplate. An internal cooling water system stabilizes the temperature of the diode pump and the vanadate crystal. The end high reflecting mirror is mounted on the piezo which translates the end mirror of the laser to maintain the optimum frequency overlap with the tunable diode laser used as a seed laser and output coupling mirror is placed at the other end. The high reflecting mirror and output-coupling mirror of the host laser form a Fabry-Perot resonator. The Fabry-Perot cavity supports specific resonant frequencies, which are formed due to the constructive and destructive interference of counter-propagating wave inside the cavity. The spacing between the longitudinal modes[36] ($\Delta\varpi$) called Free Spectral range ($\Delta\varpi = FSR = c/2nL$, c is speed of light and n is index of refraction, and L is the physical path length of the host resonator). Most of the cavity is air (n=1), the resonator length of the cavity is 17.5 cm, and this gives the Free Spectral Range of 8.6 MHz. The full-width half-maximum (FWHM) gain curve for Nd: Vanadate can support a large number of

longitudinal modes. However, due to the mode competition the modes close to the center of the gain curve captures most of the available energy. The alignment of the cavity is first done by using a He-Ne laser without the Nd:Vanadate slab in the path. The He-Ne laser is aligned with the two reflecting mirrors such that the incident and reflected beam are collinear. Now the Nd:Vanadate slab is placed in to the path of the laser and adjusted so that the He-Ne incident and reflected paths remain undisturbed. This ensures that the cavity mode is aligned with a TIR in the crystal and not with an ASE mode.

Q-switching is the next step, this is a standard design and details of its operation can be found in most laser texts [37]. A calcite polarizer, quarter-wave plate and Pockels cell (Cleveland Crystals Model IPD-2545R) is used for Q-Switching. The Polarizer is oriented in the beam path to pass the vertically polarized light, which is parallel to the Nd:Vanadate C-axis. The Q-switch is in the cavity to inhibit lasing while the diode lasers pump the vanadate crystal. Because the vanadate upper state lifetime is on the order of 50 μsec pumping times in excess of 50 μsec will not yield higher stored energy. For this reason the diode lasers pulse is 50 μsec in duration. During this time the Q-switch is set to inhibit lasing. After the 50 μsec period, the Q-switch is turned on with less than 1 nsec risetime and a high energy pulse is emitted from the cavity.

Injection seeding[38,39] is the next operation to achieve single longitudinal mode operation of Nd:YVO_4 pulsed laser by injecting a very narrow linewidth, continuous-wave (CW) seed laser in to the pulsed laser cavity when the Q-switch opens. It is very important that the injected radiation must be orders of magnitude

more than any spontaneous noise emission present in the laser cavity. The cw single mode YAG laser is used as the injection seeder in our experiment. The seed laser frequency is selected to be within the bandwidth of the pulsed laser cavity mode, so that a Q-switched pulse will be generated more rapidly out of this seed emission than that out of the background spontaneous noise emission. Thus, all the energy stored in a homogeneously broadened gain element (Nd:Vanadate) is depleted by the pulse from the seed laser emission, resulting in single frequency output from the pulsed laser.

Frequency control and stabilization of the Nd:Vanadate laser by using a seed laser is an important consideration. The standard approach is first to stabilize the seed laser frequency and then achieve frequency overlap with the Nd:Vanadate slab by temperature tuning the crystal, as the temperature of the Nd:Vanadate slab effects the frequency. The frequency of the seed laser is also temperature tunable. By changing the temperature (W1 and W2 controls inside the seed laser control box) of the seed laser crystal, its output can be tuned to the center of the Nd:Vanadate laser gain curve, this provides the most effective and stable seeding and also the highest seeded output power from the host laser.

The high reflecting end mirror mounted on the piezoelectric element in the cavity provides a way to lock the frequency of the cavity mode to the seed frequency. This provides a slow form of frequency control for the host laser such that it maintains roughly the same temperature in day-to-day operation. This also maintains the gain center of the host laser at a fixed point.

Figure 3.3 shows the experimental setup of Injection seeded diode pumped Nd:Vanadate laser system. Minimizing the Q-switch build-up time is the parameter employed to properly translate the piezo for precise frequency overlap with the seed laser. By centering the seeder output on the host laser output using these mirrors, and then fine-tuning mirrors to minimize the Q-switch build-up time, the spatial overlap can be optimized. In practice the cavity was not locked to the seed laser as we noticed effective seeding without it.

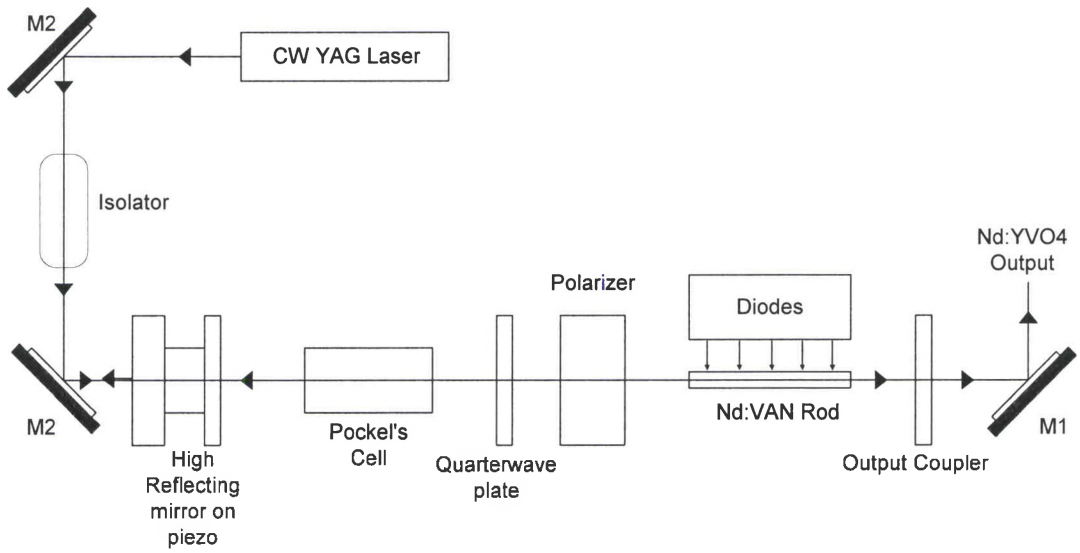

Figure 3.3 - Injection seeded Nd:Vanadate Host laser system, M1 = aluminum mirror, Output Coupler - NIR mirror (HT 1.064, 3.3 microns and HR 1.57 micron, AR 1.064 micron).

After aligning all these optics for optimum operation, output power is found to be 500 μJ/pulse. The pump has horizontal 1/e field beam diameter of 230 microns. Figure3.4 shows the variation of output power with vanadate slab temperature. This homebuilt Q-switched injection seeded Nd:Vanadate laser, as described in this section, operating at a repetition rate of 1khz is used as a pump for both the OPG stages.

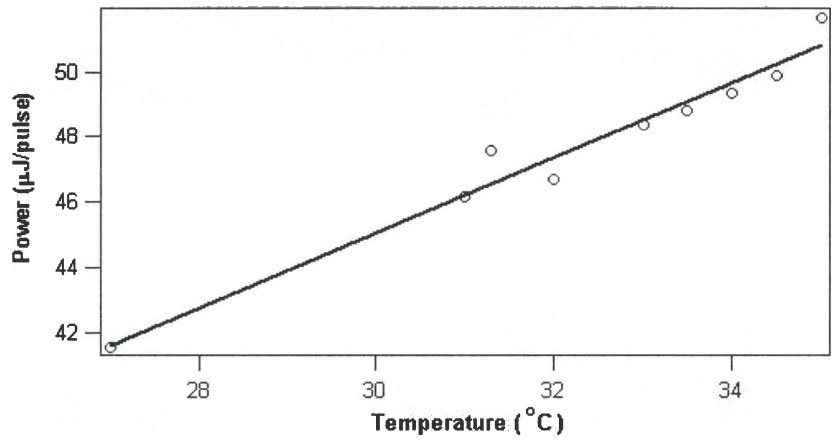

Figure 3.4 – 1064 nm power variation as a function of temperature of the Nd:Vanadate slab.

3.3 OPG setup

The Q-switched injection seeded PPLN OPG setup discussed here is based on the design developed by Powers *et.al.* [4]. This method provides broad tunability, narrow linewidth, and complete spectral coverage with in the tuning range with high conversion efficiency. In order to use this for both OPG stages, the pump beam is divided into primary and secondary pump beams with a halfwave plate and polarizer for variable partitioning of pump energy between the two OPG stages. The Primary and secondary pump beams have the same energy at the entrance of the PPLN. Pump beam is focused using a 10cm lens to have a beam waist of 230 microns at the center of the PPLN crystal in both the OPG stages. The crystals used for both the stages have single grating periodicity of 29.75 microns and have antireflection coatings at 1.064 micron and 1.5 micron.

An OPG generates a broad spectral bandwidth with high efficiency. To control the bandwidth, this OPG is seeded with a diode laser which can be tuned across the entire OPG gain bandwidth. Since the bandwidth of this is large, we

can quickly tune over this range. Tuning one or both of the OPG and then mixing these outputs in a DFG crystal generate tunable THz over the same range. The modeling of the THz wave generation shows that for difference frequency generation using the available PBG structure one laser is at 1518.87 nm and other laser could be tuned around this wavelength. For the first OPG the diode laser is operated at 1518.87 nm. The PPLN crystals were placed on the mounts with temperature-controlled heater. Temperature control is used to suppress the photorefractive effects and to tune the wavelength. At room temperature broadband spectrum output of the first stage OPG has a band gain not centered on the required wavelength i.e., 1518.87 nm. Initially to check the OPG operation the seeding is performed with the seed at 1550.25 nm by increasing the PPLN temperature to 100°C. The seeded output of the first stage OPG generated a narrow linewidth centered on 1550.25 nm. Seeded and unseeded output spectrum of the first stage OPG is as shown in the Figure 3.5 and the effect of injection seeding Nd: Vanadate pump laser with cw YAG laser on the output of single stage OPG is shown in Figure 3.6.

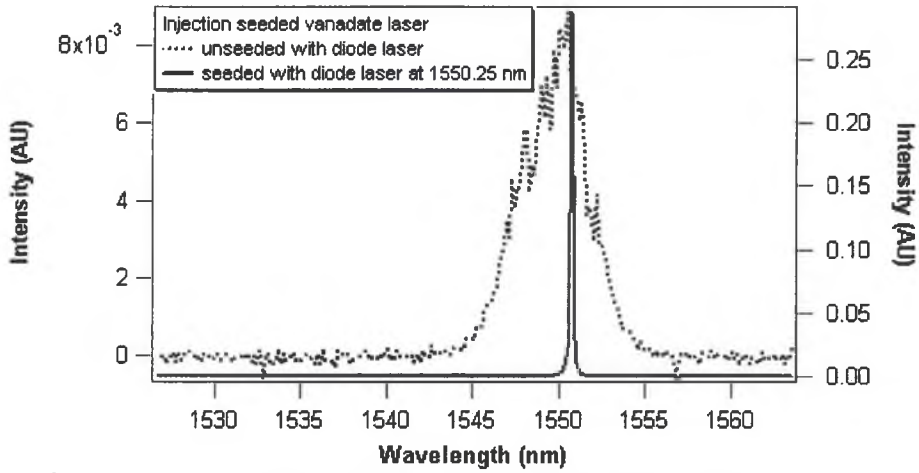

Figure 3.5 - Seeded and unseeded spectrum of the first stage optical parametric generation (OPG).

As mentioned above, one of the OPG outputs should be within the PBG defect bandwidth i.e., at 1518.87 nm. This can be achieved by using a different PPLN periodicity and seeding with the tunable diode laser. The next step is to generate THz radiation using a nonlinear crystal. Next section discusses about the THz wave generation setup using a PBG crystal as a nonlinear medium.

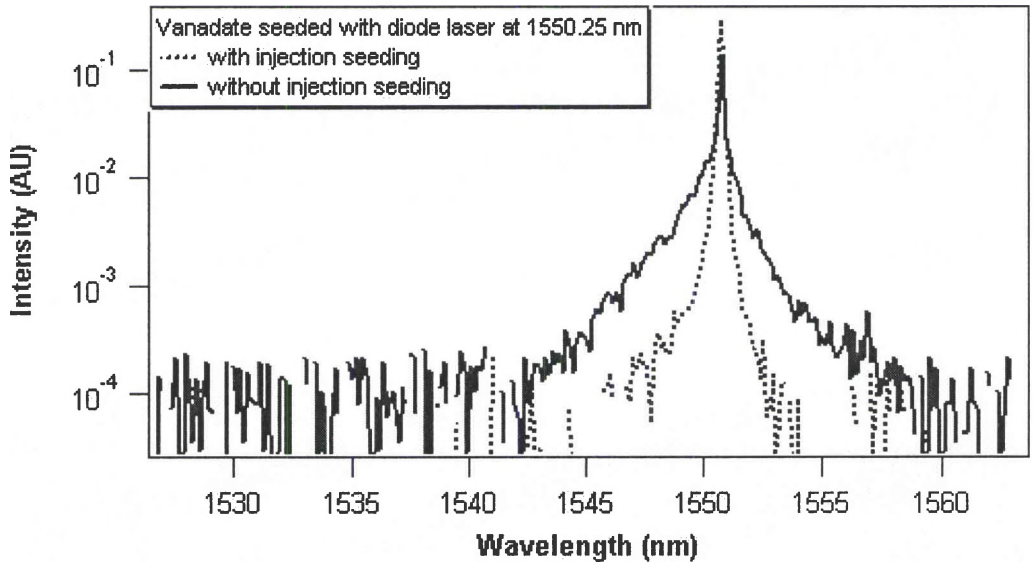

Figure 3.6 – Effect of injection seeding Nd: Vanadate pump laser with cw YAG laser on the output of single stage OPG.

3.4 Terahertz-wave generation setup

The source for the THz-wave generation is the output of seeded OPG's, the arrangement is as shown in the Figure 3.7. The two signal beams from OPG's are focused on to the PBG sample. As mentioned in chapter 2, the PBG sample used in the experiment has 18 periods of GaAs/AlAs layers and 22 periods of AlAs/GaAs layers, each period is made of 2 quarter-wave thickness layers. The thickness of GaAs layers is 112.42 nm and 130.45 nm for the AlAs layers. The GaAs defect layer has a thickness of 1,349 nm deposited on a GaAs

substrate of infinite thickness. The transmission through the available Photonic Band Gap (PBG) crystal measured using tunable cw diode laser is shown in the Figure 2.12.

We initially made the THz radiation setup in the laboratory only with single OPG stage and the PBG sample. The seeded output spectrum of the OPG has a narrow linewidth signal, but even so this bandwidth has a set of frequencies, which when focused on to the PBG crystal will undergo nonlinear processes and generate difference frequency of the signals within the narrow bandwidth. We obtained a narrow linewidth of 0.1 cm^{-1} which potentially translates into a 3GHz bandwidth signal. To detect this signal we tried a preliminary experiment using a network analyzer. The network analyzer is capable of detecting signals up to 20 GHz, and our thought was that we could see the 3 GHz signal using this device. However, spurious signals, most likely from the Q-switch made this measurement too uncertain. We believe that this approach could work if the network analyzer had a time-gating capability.

Another approach is to use a traditional nonlinear optical crystal. Continuously tunable, and coherent terahertz radiation in the range of 56.8-1618 μm (0.18-5.27 THz) based on collinear phase-matched difference frequency generation in a GaSe crystal and radiation in the ranges of 66.5-300μm (1.0-4.51 THz) and 72.7-237μm (1.26- 4.1 THz) for two configurations of phase-matched difference-frequency generation in Zinc germanium phosphide is demonstrated by Ding *et. al.,* the set up with GaSe crystal has only one tunable

source and the other source is fixed (pumped by laser with duration, 5ns; pulse energy, 3mJ; repetition rate, 10Hz).

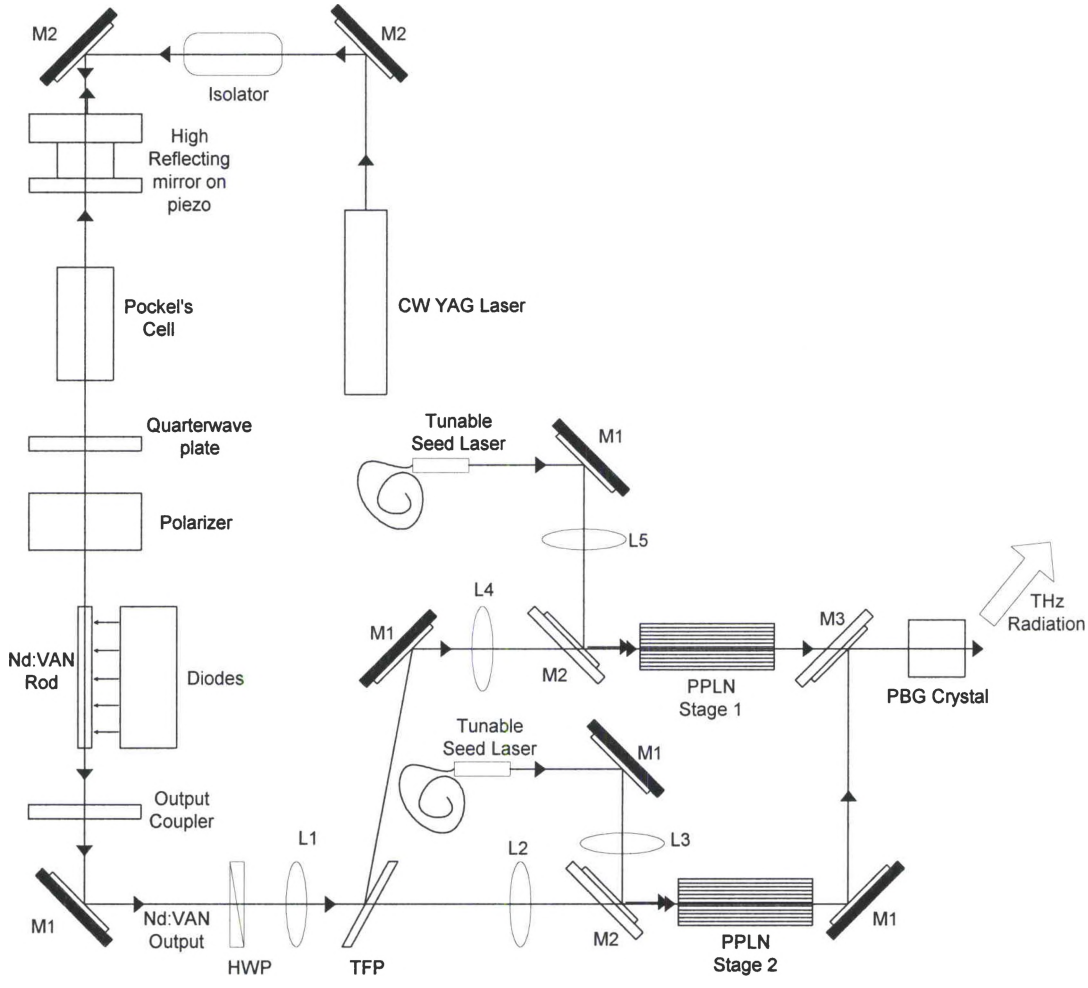

Figure 3.7 - Arrangement of the THz wave generation using the Q-switched injection seeded diode pumped Nd:Vanadate laser as pump, tunable diode lasers as seed, PBG nonlinear crystal as DFG mixer.

Kawase *et. al* demonstrated another method of tunable THz generation by difference frequency generation of dual signal-wave quasi-phase matched optical parametric oscillation with periodically poled $LiNbO_3$ (PPLN) with a series of gratings in a 4-dimethylamino-N-methyl-4-stilbazolium-tosylate (DAST) nonlinear crystal. They have demonstrated tunable THz generation of 120 to 160 micron by

changing the temperature of PPLN from 100° to 200°C. Our method is similar to that demonstrated by Ding *et. al.* except ours has two easily tunable sources with 2ns pulse duration at repetition rate of 1KHz and the nonlinear medium is a PBG crystal. Figure 3.7 shows the overall experimental arrangement for the THz wave generation. Figures 3.8 and 3.9 show the pictures of the experimental setup of the injection seeded diode pumped solid state Nd:YVO_4 home built pump laser system and the two OPG stages respectively.

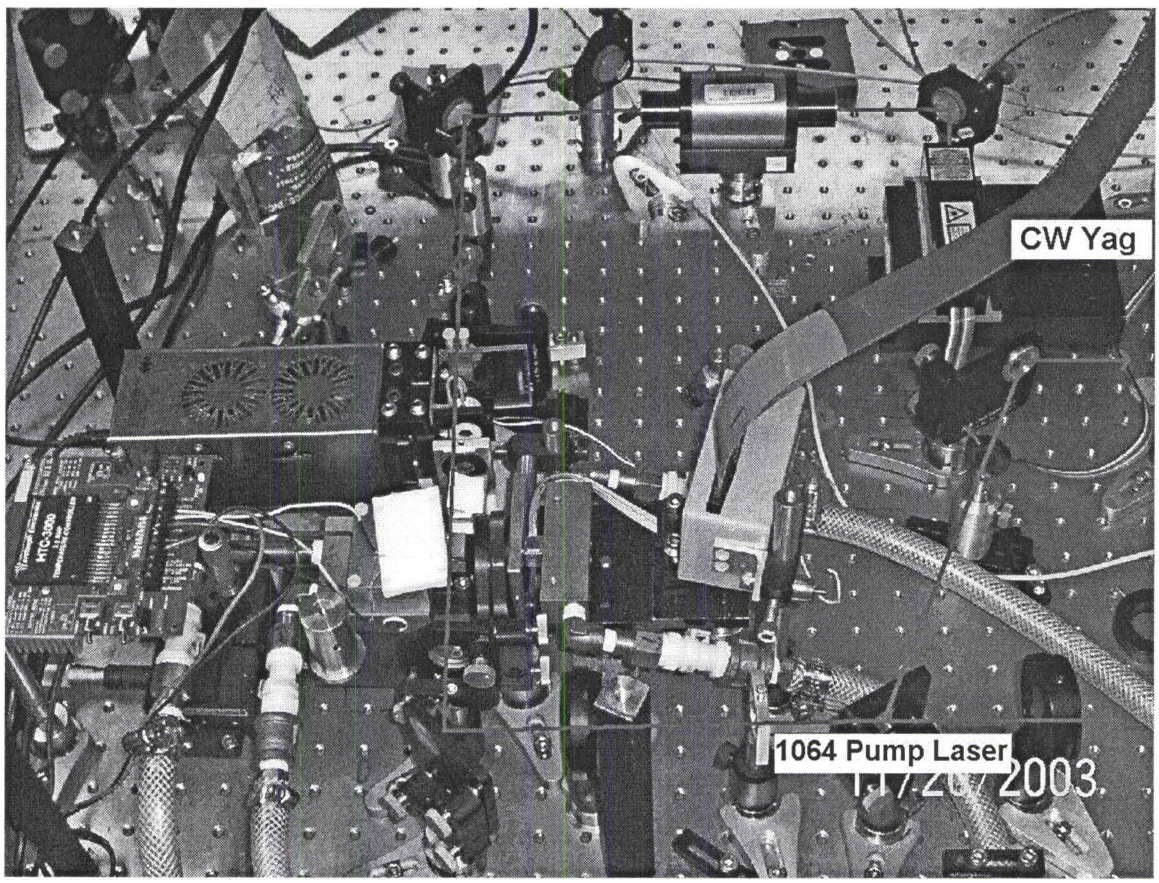

Figure 3.8 – Picture of the experimental setup for the injection seeded diode pumped solid-state Nd:YVO_4 laser. CW YAG laser is used as Injection seeder.

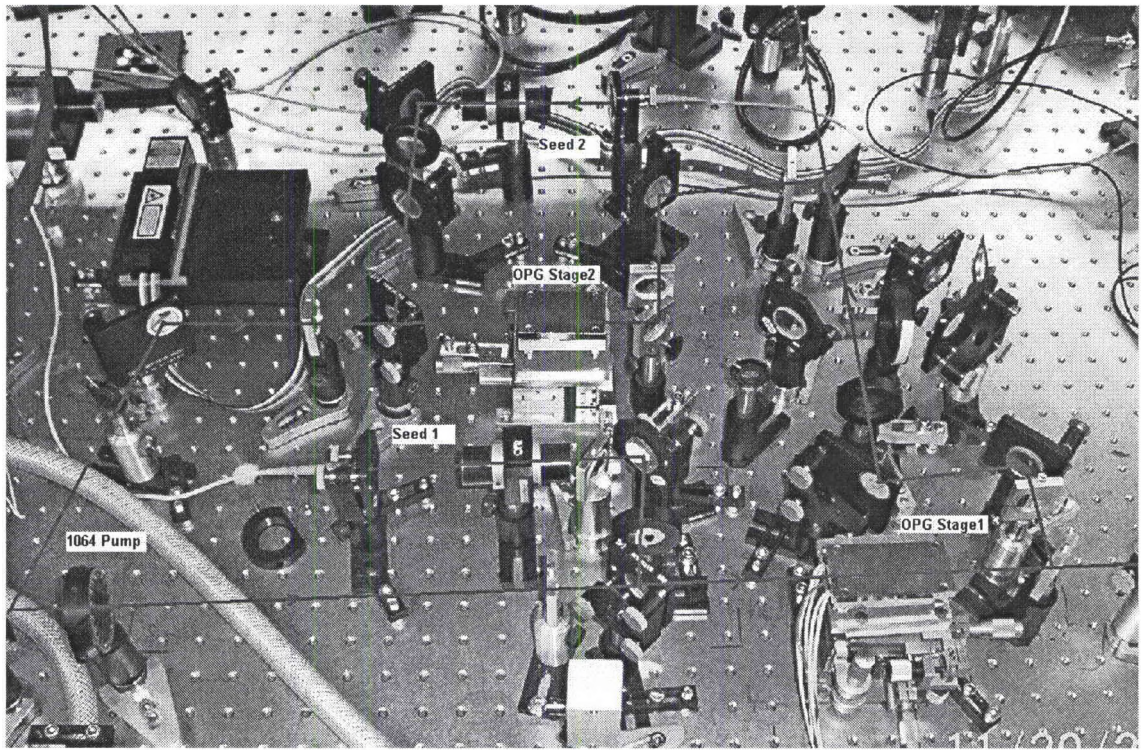

Figure 3.9 – Picture of the experimental setup for the two Optical Parametric Generators (OPG's). Tunable diode laser is used for the OPG seeding in either case.

3.5 THz-Wave Detection

A Bolometer will be used for the detection of the THz signals along with the other electronic components like preamplifiers, gated integrators and boxcar averagers. Low temperature silicon bolometers consist of a doped silicon element supported in a vacuum by lead wires attached to a cooled substrate. These bolometers approach the sensitivity limits of thermal detectors when cooled to liquid helium temperatures (less than 4.2 K).

To retain high performance at longer wavelengths detector design can be optimized based on the application. Adjusting the detector geometry, size, operating temperature (To), thermal time constant (τ), and thermal conductance (G) allows one to customize to specific design requirements. Lowering the

operating temperature improves the detector performance. Optimized material exists for bolometers operating at 4.2K, 2.0K, 1.5K, 1.2K and 0.3K. As the operating temperature decreases, greater care is given to limiting the effect of incident background radiation. Accordingly bolometers are usually mounted with cooled filters, radiation baffles, or field optics. Background limited noise performance is achievable for a wide range of applications. Bolometers available in the market have a spectral range of 2 μm to 3000 μm (0.1 THz – 150 THz). Operating temperature ranges from 0.3 to 4.2K, with an efficiency of 100% for wavelengths below 200 μm (i.e., above 1.5THz).

New designs now make it possible to construct small-scale bolometer arrays. Performance of the array unit cell is equivalent to that of a discrete bolometer. Discrete bolometers are supplied in either a "side-looking" or "down-looking" configuration. Custom discrete designs are frequently developed

Other electronic components that should be used for the signal conditioning are preamplifier, gated integrator, and Boxcar averager. We are using HD-3 bolometer (Infrared Laboratories Inc.) and LN-6C preamplifier, which has high input impedance (1000MΩ), low noise ($5nV/Hz^{½}$). The preamplifier is an ideal device for most cooled detectors requiring voltage-mode amplification. First amplifier stage is located on the cold work surface near the detector. Microphonics, stray capacitance, and other problems associated with long leads and high impedance are minimized with this system.

Gated integrators and boxcar averagers (also called Chopped Signal Integrators or Phase Sensitive Detectors) are used to recover fast, repetitive,

analog signals with time scales of 100's of picoseconds to 100's of microseconds. A time "gate" with a certain width is generated by the set delay from a trigger. A gated integrator amplifies and integrates the signal present during the gate is 'on' subtracting the noise or interference that may be present during the other time. The output of the gated integrator is averaged using a boxcar averager over many shots of the experiment. Signal processing modules can be used to display the signal on the computer. We have used the network analyzer for detecting the generated radiation as a preliminary detection process. In future, silicon bolometer will be used for the detection of the generated THz radiation.

3.6 Summary

We have demonstrated the building of the Q-switched injection seeded diode pumped Nd:Vanadate solid state laser and explained the operation and results of the diode pumping, cavity alignment, Q-switching, and injection seeding. We obtained the pump output at KHz repetition rate and good beam characteristics with 500 μJ/pulse energy. We explained the laboratory arrangement of OPG's using PPLN, and the THz detection method using the bolometer and other signal conditioning equipment.

CHAPTER 4
CONCLUSION AND FUTURE DIRECTIONS

This thesis has reported the modeling and the laboratory setup for the generation and detection of the tunable THz radiation. We have explained from the model the effect of the PBG structure and the incident field angle on the bandwidth, enhancement, and tunability of the THz radiation. Thus generated, coherent, tunable, reliable, and economical THz sources could be used for various applications like THz imaging, THz spectroscopy, wireless communications, and millimeter wave radar, just to name a few.

Chapter 1 explains the importance of this thesis work. Chapter 2 reports the modeling of the enhanced tunable THz-wave generation in PBG structures. We demonstrated the effect of the number of layers, the refractive index contrast of the PBG sample and the angle tuning of the input fields on the bandwidth, intensity, and tunability of the signal. THz radiation power conversion is presented.

Chapter 3 reports the laboratory setup for the THz-wave generation and detection. This chapter covered the operation and building of the injection seeded diode pumped Nd:YVO_4 pump laser system, Optical Parametric Generation (OPG) setup, and the detection of the generated THz signal using the Si-bolometer. The future work is to try different nonlinear optical crystals like PBG

structures, GaSe, and GaN for the terahertz-wave generation and setting up a THz-wave detection system.

REFERENCES

[1] T.W. Crowe, T. C. Grein, R. Zimmermann, and P. Aimmermann, "Progress toward solid-state local oscillators at 1THz," IEEE Microwave Guided Wave Lett. **6**, 207-208 (1996).

[2] P. R. Smith, D. H. Auston, and M. C. Nuss, "Subpicosecond photoconducting dipole antennas," J. Quantum Electronics **24**, 255-260 (1988).

[3] P. K. Benicewicz, A. J. Taylor, "Scaling of terahertz radiation from large-aperture biased InP photoconductors," Opt. Lett. **18**, 1332-1334 (1993).

[4] Piestrup M. A., Flemming R. N., "Continuously tunable submillimeter wave source," Appl. Phys. Lett. **26**, 418-419 (1975).

[5] H. Minamide, K. Kawase, K. Imai, A. Sato, H. Ito, "A continuously tunable ring-cavity THz-wave parametric oscillator," Rev. Laser Eng. **29**, 744-(2001).

[6] A. Sato, K. Imai, K. Kawase, h. Minamide, S. Wada, H.Ito, "Narrow-linewidth operation of a compact THz-wave parametric generator system," Opt. Comm. **207**, 353 (2002).

[7] M. Bass, P. A. Franken, J. F. Ward, G. Weinreich, "Optical Rectification," Phys. Rev. Lett. **9**, 446-448 (1962).

[8] K. H. Hang, P. L. Richards, Y. R. Shen, "Generation of far-infrared radiation by picosecond light pulses in $LiNbO_3$," Appl. Phys. Lett. **19**, 320-323 (1971).

[9] L. Xu, X. C. Zhang, and D. H. Auston, "Terahertz beam generation by femtosecond optical pulses in electro-optic materials," Appl. Phys. Lett. **61**, 1784-1786 (1992).

[10] S.L. Chuang, "Optical rectification at semiconductor surfaces," Phys. Rev. Lett. **68**, 102-105 (1992).

[11] R. I. Aggarwal, B. Lax, H. R. Fetterman, P. E. Tannenwald, B. J. Clifton, "Cw generation of tunable narrow-band far-infrared radiation," J. Appl. Phys. **45**, 3972-3974 (1974).

[12] E. R. Brown, K. A. McIntosh, K. B. Nichols, and C. L. Dennis, Appl. Phys. Lett. **66**, 285-290 (1995).

[13] A. M. Weiner and D. E. Leaird, "Generation of terahertz-rate trains of femtosecond pulses by phase only filtering," Opt. Lett. **15**, 51-53 (1990).

[14] A. Tredicucci, F. Capasso, C. Gmachi, D. L. Sivco, A. L. Hutchinson, A. Y. Chao, "High performance interminiband quantum cascade lasers with grades superlattices," Appl. Phys. Lett. **73**, 2101-2103 (1998).

[15] D. Grischkowsky, S. Keiding, M. Van Exter, and Ch. Fattinger, "Far-infrared time domain spectroscopy with terahertz beams of dielectrics and semiconductors," J. Opt. Soc. Am. B. **7**, 2006-2015 (1990).

[16] B. B. Hu, M. C. Nuss, "Imaging with terahertz waves," Opt. Lett. **20**, 1716-1718 (1995).

[17] R. A. Cheville, D. Grischkowsky, "Time domain terahertz impulse ranging studies," Appl. Phys. Lett. **67**, 1960-1962 (1995).

[18] W. Sha, J. Rhee, T.Norris, and W. J. Schaff, "Transient carrier and field dynamics in quantum-well parallel transport: From the ballistic to the quasi-equilibrium regime," IEEE J. Quantum Electronics **28**, 2445-2455 (1992).

[19] Brener, P. C. M. Planken, M. C. Nuss, M. S. C. Luo, S. L. Chuang, L. Pfeiffer, D. E. Leaird, A. M. Weiner, "Coherent control of terahertz emission and carrier populations in semiconductor structures," J. Opt. Soc. Am. B **11**, 2457-2469 (1994).

[20] D. R. Dykaar, and S. L. Chuang, "Terahertz electromagnetics pulse generation, physics, and applications: introduction," J. Opt. Soc. Am. B **11**, 2454-2456 (1994).

[21] A. Godone, C. Novero, "The magnesium frequency standard," Metrologia **30**, 163-181 (1993).

[22] Yan-quing Lu, Min Xiao, Gregory J. Salamo. J. Of Quantum Electronics **38**, 481-485 (2002).

[23] M. Scalora, M.J. Bloemer, A.S. Manka, J.P. Dowling, C.M. Bowden, R. Viswanathan, J.W. Haus. Phys. Rev. A. **56**, 3166-3174 (1997).

[24] O. S. Heavens, "Optical Properties of thin solid films," Dover Publications, 46-90 (1965).

[25] Steven G. Johnson, John D. Joannopoulos, "Photonic crystals – the road from theory to practice," Kluwer Academic Publishers (2002).

[26] J. Shikata, K. Kawase, K.Karino, T. Taniuchi, and H. Ito, "Tunable Terahertz wave Parametric Oscillators Using $LiNbO_3$ Crystals," *IEEE Transactions on Microwave Theory and Techniques* **48**, 653-661 (2000).

[27] K.Kawase, T. Hatanaka, H. Takahashi, K. Nakamura, T. Taniuchi, and H. Ito, "Tunable terahertz-wave generation from DAST crystal by dual signal-wave parametric oscillation of periodically poled lithium niobate," Opt. Lett. **25**, 1714-1716 (2000).

[28] Efficient, tunable, and coherent 0.18-5.27-THz source based on GaSe crystal," Opt. Lett. **27**, 1454-1456 (2002).

[29] Wei Shi and Yujie J. Ding, "Continuously tunable and coherent terahertz radiation by means of phase-matched difference-frequency generation in zinc germanium phosphide", Appl. Phys. Lett. **83**, 848-850 (2003).

[30] P. E. Powers, K. W. Aniolek, T. J. Kulp, B. A. Richman, and S. E. Bisson, "Priodically poled lithium niobate optical parametric amplifier seeded with the narrow-band filtered output of an optical parametric generator," Opt. Lett. **23**, 1886-1888 (1998).

[31]A. J. Alcock, and John E. Bernard, "Diode-Pumped Grazing Incidence Slab Lasers," IEEE J. of Selected Topics in Quantum Electronics **3**, 3-8 (1997).

[32] J. E. Bernard, A. J. Alcock, "High-repetition-rate, diode-pumped Nd:YVO_4 laser," Opt. Lett. **32**, 2085-2086 (1993).

[33] J. E. Bernard, A. J. Alcock, "High-efficiency diode-pumped Nd:YVO_4 slab laser," Opt. Lett. **18**, 968-970 (1993).

[34]J. R. O'Connor, "Unusual crystal-field energy levels and efficient laser properties of YVO_4:Nd," Appl. Phys. Lett. **8-9**, 407-409 (1966).

[35] K.Chan, "Multi-Pass laser-diode-pumped Nd:YAG amplifier: design," Appl. Opt, **26**, 3177-3179 (1987).

[36] A. E. Siegman & R. Arathoon, "Modes in Unstable Optical Resonators and Lens Waveguides", IEEE J. Quantum Electronics **3**, 156-163 (1967).

[37] Eugene Hecht, Alfred Zajac, "Optics", 264, Addison-Wesley Publishing Company.

[38] Johnson, Herbst, Scerbak, and Kane, "Injection Seeded High Power Laser System", Lasers 87 Conference.

[39] R. L. Schmitt and L. A. Rahn, "Diode-laser-pumped Nd:YAG laser injection seeding system", Appl. Opt. **25**, 629-633 (1986).